The Effect of Temperature on the London Dispersive and Lewis Acid-Base Surface Energies of Polymethyl Methacrylate Adsorbed on Silica by Inverse Gas Chromatography

Tayssir Hamieh [1,2] (iD)

1 Faculty of Science and Engineering, Maastricht University, P.O. Box 616,
6200 MD Maastricht, The Netherlands; t.hamieh@maastrichtuniversity.nl
2 Laboratory of Materials, Catalysis, Environment and Analytical Methods (MCEMA), Faculty of Sciences,
Lebanese University, Beirut P.O. Box 6573/14, Lebanon

Abstract: Inverse gas chromatography at infinite dilution was used to determine the surface thermodynamic properties of silica particles and PMMA adsorbed on silica, and more particularly, to quantify the London dispersive energy γ_s^d, the Lewis acid γ_s^+, and base γ_s^- polar surface energies of PMMA/silica composites as a function of the temperature and the recovery fraction θ of PMMA. The polar acid-base surface energy γ_s^{AB} and the total surface energy of the different composites were then deduced as a function of the temperature. In this paper, the Hamieh thermal model was used to quantify the surface thermodynamic energy of polymethyl methacrylate (PMMA) adsorbed on silica particles at different recovery fractions. A comparison of the new results was carried out with those obtained by applying other molecular models of the surface areas of organic molecules adsorbed on the different solid substrates. An important deviation of these molecular models from the thermal model was proved. The determination of γ_s^d, γ_s^+, γ_s^-, and γ_s^{AB} of PMMA in both the bulk and adsorbed phases showed an important non-linearity variation of these surface parameters as a function of the temperature. The presence of maxima in the curves of $\gamma_s^d(T)$ highlighted the second-order transition temperatures in PMMA showing beta-relaxation, glass transition, and liquid–liquid temperatures. These three transition temperatures depended on the adsorption rate of PMMA on silica. The proposed method gave a new relation between the recovery fraction of PMMA and its London dispersive energy, showing an important effect of the temperature on the surface energy parameters of the adsorption of PMMA on silica. A universal equation relating $\gamma_s^d(T, \theta)$ of the systems PMMA/silica to the recovery fraction and the temperature was proposed.

Keywords: hamieh thermal effect; London dispersive surface energy; polar surface energy; recovery fraction; transition temperatures

1. Introduction

The estimation of the London dispersive and acid-base surface energies of solids, oxides, and polymers [1–14] is of crucial importance in many industrial processes, such as adhesion, paints, coatings, corrosion, chemical reactions, adsorption, and catalysis. The most used technique to determine these surface parameters was inverse gas chromatography (IGC) at infinite dilution. The net retention time and volume of organic solvents adsorbed on solid surfaces, experimentally obtained by IGC, are directly correlated to the surface thermodynamic properties of solid materials, such as the London dispersive $\gamma_s^d(T)$ and polar $\gamma_s^p(T)$ components of the surface energy of solid particles as a function of the temperature. The interesting IGC technique used to characterize the surface and polar characteristics of materials was applied more particularly to determine the London dispersive energy of lignocellulosic fibers [15] based on works of Jacob et al. [16], Carvalho et al. [17], Chtourou et al. [18], Dorris and Gray [19], and Donnet et al. [20,21].

Gamble et al. [22] determined that the surface energy characteristics of a drug substance coated with two grades of silicon dioxide were studied by IGC using the Dorris and Gray approach. The IGC technique was used by Balard et al. [23] to determine the surface properties of milled graphites, by Bogillo et al. [24] to evaluate the surface-free energy components for heterogeneous solids, and by Das et al. [25,26] to study the surface energy distributions of lactose and pharmaceutical powders. The adsorption of n-alkanes at zero surface coverage on cellulose paper and wood fibers [19,27] and solid surface polarity [28] using IGC at infinite dilution were studied. Feeley et al. [29] studied the surface properties and flow characteristics of salbutamol sulphate, and the surface energy characteristics of micronized materials were determined [30]. The same technique was also used to measure the surface energy and high-energy sites for mixtures of crystalline and amorphous lactose [31,32]. Kołodziejek et al. [33] studied the relationship between surface properties determined by inverse gas chromatography and ibuprofen release from hybrid materials based on fumed silica, whereas Ho et al. [34–36] studied the surface energy heterogeneity of crystals with IGC. Many authors studied the surface energies of some polymers, such as tosylate functionalized poly(ethylene glycol) [37], polybutadiene/fillers [38], poly(2,2,3,3,3-pentafluoropropyl methacrylate) [39], and hyperbranched poly(ester amide) [40].

Several studies were interested in the adsorption of polymers on solid substrates or metallic oxides and their behaviors near the glass transition [41–46]. Other works were devoted to the segmental relaxation dynamics of poly(methyl methacrylate)/silica nanocomposites near and above the glass transition temperature by mechanical spectroscopy [47] and to the physical aging behavior under different adsorption conditions of PMMA chains [48–52].

In previous works [53,54], we studied the adsorption of PMMA on silica and alumina particles and the glass transition using inverse gas chromatography. However, classic chromatographic methods were used to determine the dispersive and polar-free energies of adsorbed organic molecules on the solid surfaces. In a recent study [55], the previous results were corrected using the new methodology based on the London dispersion interaction, and the new Lewis acid-base properties of PMMA/silica were obtained. The various dispersive, polar, and Lewis acid-base surface energies of the composites were not studied in the literature in light of the new thermal model.

The concept of the surface free energy γ_s of material was first introduced by Fowkes [56] and resulted from a variety of intermolecular forces, such as the hydrogen bond, metallic bond, and London dispersion interaction [57,58]. The general expression of γ_s can be given by

$$\gamma_s = \gamma_s^d + \gamma_s^p + \gamma_s^i + \gamma_s^c + \gamma_s^m \tag{1}$$

where γ_s^d is the London dispersive component of the surface energy; the symbols *p*, *i*, *c*, and *m* are, respectively, the polar (due to Debye, Keesom, hydrogen, and acid-base interactions), ionic, covalent, and metallic components of the surface energy of the material. Relation 1 can be, in general, expressed as follows:

$$\gamma_s = \gamma_s^d + \gamma_s^{nd} \tag{2}$$

where γ_s^{nd} includes all non-dispersive interaction forces. The non-dispersive component can be also symbolized by the total polar contribution γ_s^p of the surface energy.

In this paper, we used the IGC technique [35–40,59–83] at infinite dilution to determine the dispersive $\gamma_s^d(T)$ and polar $\gamma_s^p(T)$ components of the surface energy, as well as Lewis's acid-base surface energies of poly(methyl methacrylate) (PMMA) adsorbed on silica at different recovery fractions as a function of the temperature using our new approach based on the Hamieh thermal model [59–61] that gave the variations of the surface area of adsorbed organic molecules as a function of the temperature.

2. IGC Methods and Materials

The experimental values of the net retention time t_n and volume V_n of the adsorbed organic solvents on PMMA and silica were obtained from the direct measurements using inverse gas chromatography (IGC) at infinite dilution [59–83]. The London dispersive energy was determined using the concept of Fowkes based on the geometric mean of the respective values of the London dispersive components of the surface energy of the non-polar molecule γ_l^d and the solid substrate γ_s^d. The non-polar solvents generally used in the IGC technique were the n-alkanes (from n-pentane C5 to n-decane C10). The determination of $RTlnV_n$ of n-alkanes adsorbed on PMMA/silica at different temperatures will lead to the values of $\gamma_s^d(T)$ using the following relation:

$$RTlnV_n = 2\mathcal{N}a\left(\gamma_l^d\gamma_s^d\right)^{1/2} + \alpha(T) \tag{3}$$

where T is the absolute temperature of the chromatographic column containing the solid material, R is the perfect gas constant, a is the surface area of an adsorbed molecule, $\mathcal{N}$ is the Avogadro number, and $\alpha(T)$ is a constant depending only on the temperature and the solid material.

Relation 1 was used to deduce the value of γ_s^d by supposing both γ_l^d and a parameters as constants. Hamieh criticized the above approximation in several studies [59–61,81–83] by proving an important thermal effect on the surface area of organic molecules adsorbed on solid surfaces. We previously proposed different molecular models allowing for the determination of the surface areas of molecules [76], using Kiselev results, the two-dimensional Van der Waals (VDW) and Redlich–Kwong (R–K) equations, and the geometric, cylindrical, and spherical model. However, the most accurate model was based on the thermal model [59–61], which gave the expressions of the surface area $a(T)$ of organic molecules as a function of the temperature and those of $\gamma_l^d(T)$ relative to the different molecules.

A commercial Focus GC gas chromatograph apparatus (Sigma-Aldrich, St. Quentin Fallavier, France) equipped with a flame ionization detector (FID) was used in this study to obtain the net retention time and volume of different n-alkanes that were injected into a stainless-steel column (with a 2 mm inner diameter and a length of 20 cm) containing the solid particles. The temperature range varied from 30 °C to 200 °C. The same experimental procedure as those used in other studies [64–68] was applied to PMMA/silica. The used n-alkanes (pentane, hexane, heptane, octane, nonane) of a highly pure grade (99%) were purchased from a local chemical society.

The flow rate of the carrier gas (helium) was 20 mL/min, whereas the temperatures of the injector and detector were fixed at 200 °C. The infinite dilution of the probes was realized with the help of 1 μL Hamilton syringes by injecting very small quantities of the vapor solvent, satisfying the limit of detection of the FID of high sensitivity to practically realize the zero-surface coverage [84]. All columns containing PMMA and silica particles were preconditioned at 130 °C overnight to remove any adsorbed water molecules or other residual impurities.

PMMA and silica solid particles with different recovery fractions of PMMA (varying from 0 to 1.0) used in this work were the same solid materials previously characterized in other studies using other chromatographic methods [53,54].

3. Experimental Results

3.1. London Dispersive Surface Energy of Silica Particles

The values of $RTlnV_n$ and $2\mathcal{N}a\left(\gamma_l^d\right)^{1/2}$ of silica particles at different temperatures are given in Tables S1 and S2 by taking into account the thermal effect of the temperature on the surface area of organic solvents. Figure 1 gives the variations of $\gamma_s^d(T)$ of silica as a function of the temperature using the Hamieh thermal model.
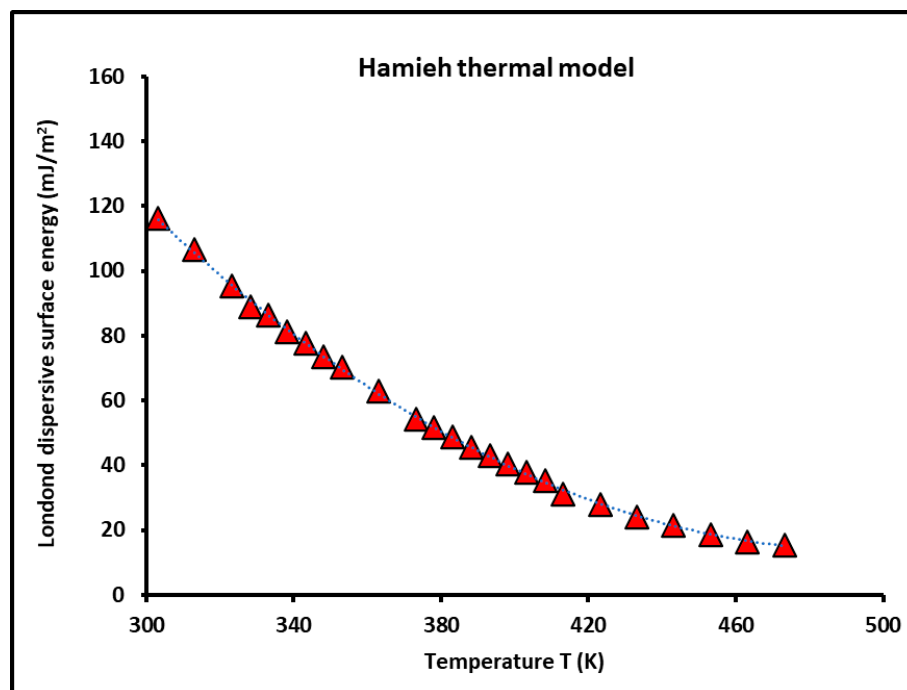
Figure 1. Evolution of the London dispersive surface energy $\gamma_s^d(T)$ (mJ/m^2) of silica particles as a function of the temperature using the Hamieh thermal model. The dotted line represents the parabolic interpolation of the variations of $\gamma_s^d(T)$ and the red triangles represent the experimental values.

Figure 1 shows that the monotonous decrease in the London dispersive surface energy of silica is not perfectly linear. The non-linear variation of $\gamma_s^d(T)$ can be approached by parabolic interpolation in this case. Equation (2) was obtained with an excellent regression coefficient ($R^2 = 0.9994$) in the studied domain of temperature as follows:

$$\gamma_s^d(T) = 2.8 \times 10^{-3}T^2 - 2.76T + 691.29 \tag{4}$$

Several molecular models of the surface area of n-alkanes were used: the geometrical model (based on the real surface area of molecules), the cylindrical molecular model (supposing a cylindrical form of molecule), the spherical model (supposing a spherical geometric form), Kiselev results, and the models using the two-dimensional Van der Waals and Redlich–Kwong equations transposed from three-dimensional space to two-dimensional space.

The comparison of this result with that obtained using other molecular models is shown in Figure 2.

The results presented in Figure 2 and Table 1 show the monotonous variations of $\gamma_s^d(T)$ of silica particles for all used molecular models with parabolic curves. However, an important deviation of all models was observed with respect to the Hamieh thermal model [59–61]. Indeed, the spherical model overestimated the values of the London dispersive surface energy of solid materials, whereas the geometric model underestimated the values of $\gamma_s^d(T)$, while the cylindrical, Kiselev, and Van der Waals models were the closest to that of the thermal model. The different molecular models did not take into consideration the thermal effect on the surface area. This incorrect assumption is the real cause of the erroneous values of γ_s^d obtained by applying the different molecular models in comparison to those obtained by the thermal model.
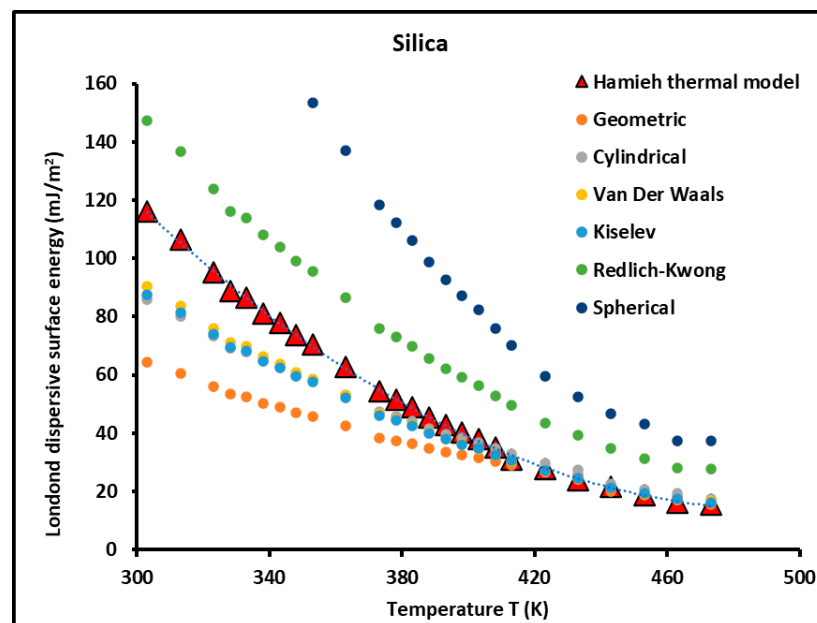
Figure 2. Variations of γ_s^d (T) of silica particles as a function of the temperature using the various models compared to the Hamieh thermal model. The dotted line represents the parabolic interpolation of the variations of $\gamma_s^d(T)$ obtained by the Hamieh thermal model.

Table 1. Values of γ_s^d (T) (in mJ/m^2) of silica particles as a function of the temperature using the various models and the new Hamieh thermal model.

T (K)	Hamieh Thermal Model	Geometric	Cylindrical	Van Der Waals	Kiselev	Redlich–Kwong	Spherical
303.15	116.29	64.36	85.89	90.32	87.55	147.35	253.33
313.15	106.48	60.64	80.22	83.74	81.35	136.6	232.09
323.15	95.37	55.98	73.36	75.97	73.97	123.92	207.92
328.15	88.87	53.59	69.12	71.26	69.48	116.24	193.73
333.15	86.42	52.4	67.96	69.78	68.13	113.83	188.45
338.15	81.23	50.33	64.91	66.22	64.86	108.02	177.77
343.15	77.81	48.84	62.64	63.73	62.39	103.95	169.66
348.15	73.68	47.11	60.05	60.79	59.6	99.16	160.63
353.15	70.45	45.91	58.16	58.57	57.51	95.54	153.56
363.15	62.86	42.65	53.3	53.1	52.31	86.61	136.95
373.15	54.33	38.5	47.41	46.68	46.14	76.13	118.24
378.15	51.68	37.5	45.8	44.8	44.37	73.06	112.41
383.15	48.93	36.39	44.05	42.8	42.48	69.8	106.33
388.15	45.55	34.78	41.72	40.22	40.01	65.6	98.87
393.15	43.01	33.48	39.78	38.08	37.96	62.11	92.62
398.15	40.28	32.5	38.22	36.29	36.27	59.19	87.27
403.15	38.02	31.63	36.78	34.62	34.69	56.47	82.25
408.15	35.25	30.3	34.81	32.47	32.62	52.95	76.13
413.15	31.13	29.07	32.93	30.41	30.64	49.59	70.32
423.15	27.85	26.93	29.55	26.65	27.04	43.46	59.71
433.15	23.93	25.9	27.45	24.21	24.7	39.48	52.37
443.15	21.53	19.93	22.67	21.38	21.41	34.88	46.62
453.15	18.74	18.79	20.75	19.11	19.26	31.17	43.1
463.15	16.34	18.13	19.28	17.23	17.49	28.11	37.52
473.15	15.47	15.65	17.5	16.96	16.16	27.66	37.41

This large deviation (Table 1) resulted from the fact that the effect of the temperature on the surface area of molecules was neglected in the above models. The thermal model gave different expressions of the variations of the surface area of organic molecules as a function of the temperature, whereas the other molecular models supposed all surface areas as constant. Therefore, only the results of the thermal model can be considered as accurate. The closest results to those of the thermal model were obtained by the Van der Waals model, perhaps because this model used the critical coordinates proper of each molecule. The Kiselev and cylindrical models gave similar results as those of Van der Waals with a deviation approaching 30%. The hypothesis that these above models used the cylindrical geometry of the various n-alkanes was a real hypothesis and took into account the adsorption position of such molecules but neglected, at the same time, the thermal effect. The maximum deviation was obtained with the spherical model due certainly to the use of the largest approximation considering a spherical geometry for n-alkanes, and these molecules exhibit generally linear forms.

3.2. Study of $\gamma_s^d(T)$ of PMMA and PMMA/Silica Composites

Figure 3 brings together the results of the London dispersive surface energy of PMMA particles obtained by the various applied molecular models compared to those of the thermal model. It can be observed that the results of the molecular models extremely deviate from those of the Hamieh thermal model. However, the general tendency of all drawn curves in Figure 3 and shown in Table 2 highlight the same values of the three maxima of temperatures. These three maxima showed the presence of three transition temperatures that were proved in other studies [53,54]. The beta-relaxation temperature, the glass transition, and the liquid–liquid temperatures were, respectively, obtained at 60 °C, 110 °C, and 160 °C, located on the different maxima of $\gamma_s^d(T)$, as shown in Figures 3 and 4 and Table 2 (in bold dark red). The curves obtained by the thermal model and those of the cylindrical, Kiselev, geometric, and Van de Waals models are mixed up after a temperature of 400 K.
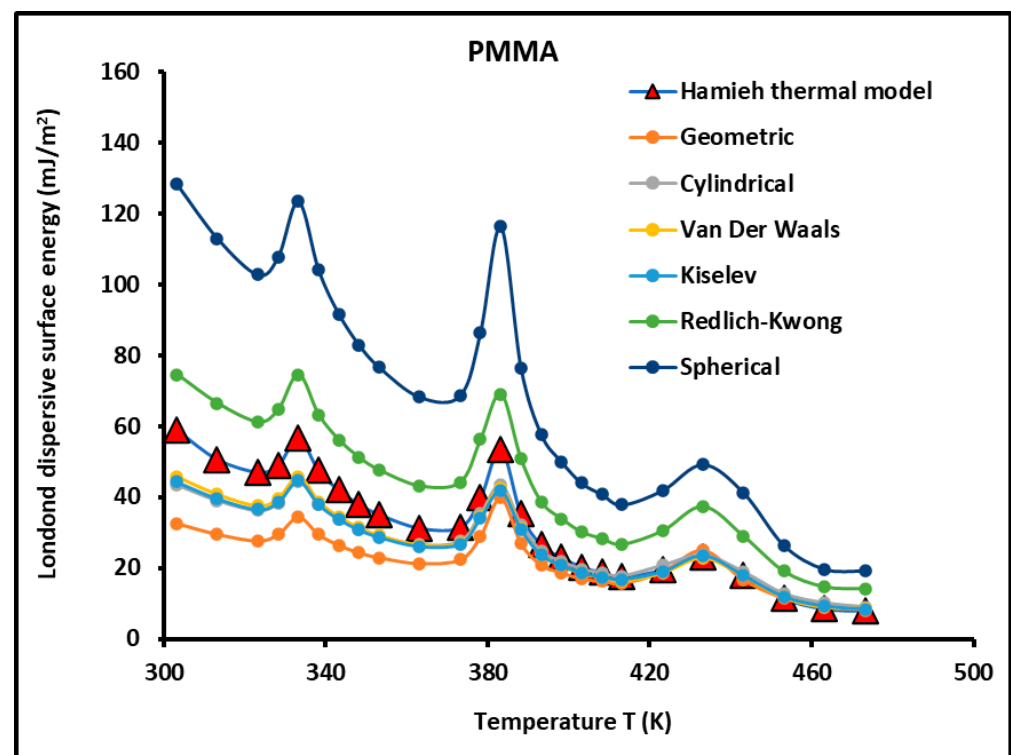

Figure 3. Variations of γ_s^d (T) of PMMA in bulk phase as a function of the temperature using the various molecular models.

Table 2. Values of $\gamma_s^d(T)$ (in mJ/m^2) of PMMA as a function of the temperature using the different models. The red bold values represent the coordinates of the maxima of $\gamma_s^d(T)$ indicating the presence of the transition temperatures of PMMA.

| T(K)	Hamieh Thermal Model	Geometric	Cylindrical	Van Der Waals	Kiselev	Redlich–Kwong	Spherical
303.15	58.87	32.58	43.48	45.73	44.32	74.61	128.26
313.15	50.68	29.5	39.03	40.75	39.58	66.47	112.94
323.15	47.11	27.65	36.23	37.53	36.54	61.23	102.73
328.15	49.08	29.49	38.44	39.65	38.66	64.69	107.82
333.15	**56.62**	**34.33**	**44.52**	**45.72**	**44.63**	**74.58**	**123.47**
338.15	47.53	29.45	37.98	38.76	37.96	63.22	104.05
343.15	42.03	26.38	33.83	34.43	33.7	56.16	91.65
348.15	38.03	24.31	30.99	31.38	30.76	51.19	82.93
353.15	35.14	22.89	29	29.22	28.68	47.66	76.6
363.15	31.31	21.23	26.54	26.45	26.05	43.14	68.21
373.15	31.53	22.34	27.51	27.09	26.78	44.18	68.63
378.15	39.80	28.87	35.26	34.49	34.17	56.26	86.57
383.15	**53.54**	**39.82**	**43.41**	**42.36**	**41.9**	**69.1**	**116.35**
388.15	35.24	26.89	32.26	31.12	30.95	50.75	76.52
393.15	26.59	20.85	24.77	23.72	23.64	38.68	57.69
398.15	23.08	18.62	21.89	20.79	20.78	33.91	50.01
403.15	20.31	16.9	19.65	18.51	18.53	30.18	43.96
408.15	18.87	16.22	18.63	17.38	17.46	28.35	40.77
413.15	17.54	15.63	17.71	16.35	16.74	26.67	37.83
423.15	19.53	18.88	20.72	18.69	18.96	30.48	41.87
433.15	**23.16**	**25.01**	**23.62**	**22.91**	**23.47**	**37.37**	**49.22**
443.15	17.91	16.58	18.85	17.79	17.81	29.01	41.27
453.15	11.48	11.5	12.71	11.71	11.79	19.1	26.4
463.15	8.58	9.51	10.12	9.05	9.18	14.76	19.71
473.15	7.93	8.04	8.98	8.68	8.29	14.16	19.16
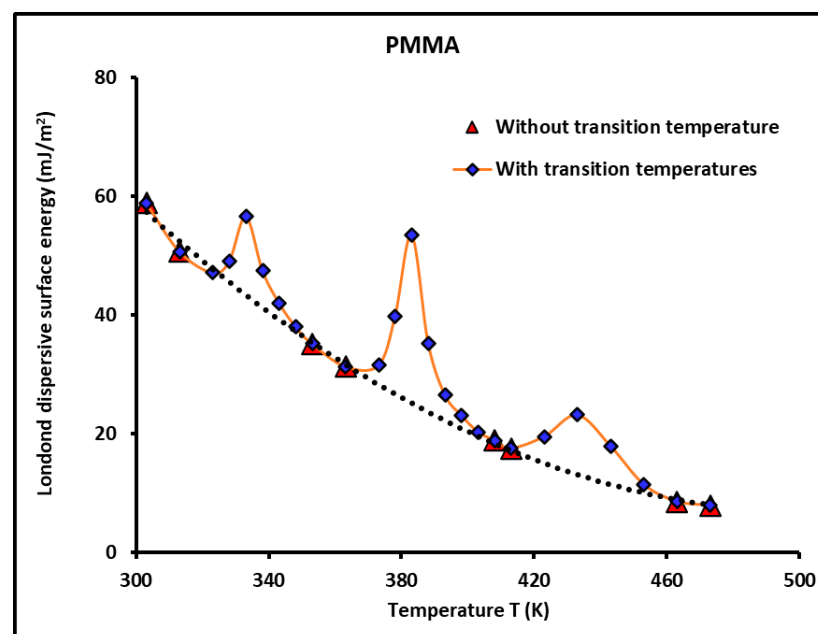
Figure 4. Variations of $\gamma_s^d(T)$ of PMMA as a function of the temperature using the Hamieh thermal model. The dashed line is relative to the curve without considering the transition phenomenon and the red line shows the three transition temperatures.

To better understand the effect of the various transition phenomena on the London dispersive surface energy, the one represented in Figure 4, the evolution of $\gamma_s^d (T)$ of PMMA as a function of the temperature using the thermal model and the corresponding curve of $\gamma_s^d (T)$ supposes that there is no transition temperature and shows the transition temperatures. The dashed line shows a parabolic monotonous decrease in γ_s^d when the temperature increases. The equation of $\gamma_s^d(T)$ of PMMA without transition temperature is given by

$$\gamma_s^d(T) = 1.2 \times 10^{-3}T^2 - 1.26T + 324.00 \tag{5}$$

A comparison with Equation (4) relative to silica particles showed that the values of $\gamma_s^d (T)$ of silica are approximately double those of PMMA without transition phenomenon. On the other hand, the comparison between the two curves in Figure 4 showed that before every transition temperature, the London dispersive surface energy of PMMA increased until it reached its maximum value relative to the transition temperature with unstable equilibrium and again decreased to join the dashed line. The variations of $\gamma_s^d(T)$ around the transition temperature are due to the intense motion and fluctuations of the chain groups of the polymer. Table 2 clarifies the values of $\gamma_s^d(T)$ when the temperature increased.

The highest non-linearity of the curves $\gamma_s^d (T)$ of PMMA was observed in all molecular models in the temperature interval [300 K; 500 K]. This non-linearity is certainly due to the presence of transition phenomena in PMMA submitted to the surface group changes when the temperature increases. All molecular models largely deviate from the thermal model. The deviation reached 300% in many cases. However, the results obtained by those models can be only considered qualitative, whereas the thermal model gave the most accurate results.

The results relative to the adsorption of PMMA on silica particles are presented in Figure 4 and Table 3 at different recovery fractions varying from $\theta = 0$ (the case of pure silica particles) to $\theta = 1.0$ (representing a monolayer of PMMA on silica). The results in Figure 5 and Table 3 clearly show the large difference in the values of the London dispersive surface energy of the PMMA/silica composites when the temperature and the recovery fraction changed. Three interesting results were detected as follows:

Table 3. Values of $\gamma_s^d (T)$ of PMMA adsorbed on silica particles as a function of the temperature at different recovery fractions from $\theta = 0.31$ to $\theta = 1.0$ using the various molecular models. The bold dark red figures are relative to the transition temperatures.

Adsorption of PMMA on Silica for θ=0.31						
T (K)	Hamieh Thermal Model	Geometric	Cylindrical	Van Der Waals	Kiselev	Redlich–Kwong	Spherical
303.15	104.37	57.76	77.09	81.07	78.57	132.24	227.37
313.15	91.30	51.99	68.78	71.80	69.75	117.13	199.00
323.15	81.98	48.12	63.06	65.31	63.59	106.54	178.75
328.15	78.95	47.09	61.39	63.31	61.73	103.28	172.15
333.15	80.44	48.78	63.26	64.95	63.41	105.95	175.41
338.15	81.52	50.51	65.15	66.46	65.09	108.41	178.40
343.15	**83.10**	**52.17**	**66.90**	**68.05**	**66.63**	**111.01**	**181.19**
348.15	73.51	47.00	59.91	60.65	59.46	98.93	160.25
353.15	64.73	42.18	53.43	53.82	52.84	87.78	141.09
363.15	53.21	36.09	45.11	44.94	44.27	73.31	115.91
373.15	43.45	30.79	37.91	37.33	36.90	60.88	94.56
378.15	41.08	29.80	36.40	35.60	35.27	58.07	89.35
383.15	39.48	29.35	35.54	34.53	34.27	56.33	85.81
388.15	40.75	31.10	37.30	35.98	35.79	58.69	88.48
393.15	45.69	35.85	42.56	40.74	40.62	66.45	99.10
398.15	**50.97**	**41.15**	**48.37**	**46.28**	**45.89**	**74.90**	**110.42**
403.15	43.24	36.00	41.84	39.38	39.46	64.23	93.55
408.15	35.25	30.10	34.52	32.17	32.33	52.47	75.41

Table 3. *Cont.*

T (K)	Hamieh Thermal Model	Geometric	Cylindrical	Van Der Waals	Kiselev	Redlich–Kwong	Spherical
Adsorption of PMMA on Silica for θ=0.31							
413.15	28.80	25.66	29.07	26.84	27.04	43.78	62.08
423.15	22.94	22.18	24.34	21.95	22.27	35.80	49.18
433.15	23.99	21.38	22.44	19.60	20.07	31.96	42.09
443.15	**27.13**	**25.13**	**28.57**	**29.95**	**26.99**	**43.95**	**62.52**
453.15	19.05	19.10	21.09	19.42	19.57	31.68	43.80
463.15	14.48	16.06	17.08	15.27	15.50	24.91	33.25
473.15	13.85	14.04	13.03	10.36	11.03	16.89	20.69
Adsorption of PMMA on Silica for θ = 0.54							
T (K)	Hamieh Thermal Model	Geometric	Cylindrical	Van Der Waals	Kiselev	Redlich–Kwong	Spherical
303.15	95.71	53.22	70.69	74.34	72.05	121.26	208.47
313.15	84.53	48.13	63.67	66.47	64.57	108.43	184.23
323.15	74.85	43.93	57.57	59.62	58.06	97.26	163.19
328.15	72.05	42.97	56.03	57.78	56.34	94.26	157.12
333.15	73.29	44.44	57.63	59.17	57.77	96.53	159.81
338.15	**76.92**	**47.65**	**61.43**	**62.71**	**61.42**	**102.29**	**168.35**
343.15	71.19	44.68	57.31	58.31	57.08	95.12	155.23
348.15	65.49	41.87	53.37	54.03	52.97	88.14	142.77
353.15	58.91	38.09	48.43	49.22	48.08	80.29	129.15
363.15	48.96	33.21	41.51	41.36	40.74	67.46	106.65
373.15	38.16	27.04	33.3	32.78	32.41	53.47	83.06
378.15	36.12	26.2	32	31.31	31.01	51.06	78.57
383.15	38.33	28.5	34.51	33.53	33.28	54.69	83.32
388.15	42.68	32.58	39.08	37.7	37.5	61.49	92.7
393.15	**52.06**	**40.83**	**48.5**	**46.42**	**46.28**	**75.72**	**112.92**
398.15	46.88	37.86	44.5	42.24	42.22	68.89	101.55
403.15	40.96	34.09	39.63	37.3	37.37	60.84	88.61
408.15	31.95	27.28	31.29	29.16	29.31	47.56	68.36
413.15	24.69	22.04	24.95	23.01	23.19	37.52	53.18
423.15	20.39	19.71	21.63	19.51	19.79	31.82	43.71
433.15	**26.55**	**23.63**	**24.79**	**21.66**	**22.18**	**35.31**	**46.51**
443.15	17.74	16.42	18.67	17.61	17.64	28.73	40.87
453.15	14.20	14.35	15.85	14.61	14.71	23.82	32.94
463.15	12.12	13.44	14.29	12.78	12.97	20.84	27.82
473.15	11.41	11.57	12.92	12.85	11.93	20.38	27.57
Adsorption of PMMA on Silica for θ = 0.83							
T (K)	Hamieh Thermal Model	Geometric	Cylindrical	Van Der Waals	Kiselev	Redlich–Kwong	Spherical
303.15	83.96	46.46	62.01	65.21	63.21	106.39	182.9
313.15	76.57	43.6	57.67	60.22	58.49	98.23	166.91
323.15	66.94	39.29	51.49	53.33	51.93	87	145.96
328.15	69.57	41.49	54.1	55.79	54.4	91.02	151.71
333.15	**74.62**	**45.24**	**58.68**	**60.25**	**58.82**	**98.29**	**162.72**
338.15	69.65	43.16	55.67	56.79	55.62	92.64	152.46
343.15	64.16	40.28	51.65	52.55	51.44	85.72	139.91
348.15	58.34	37.3	47.55	48.14	47.19	78.53	127.2
353.15	52.02	33.95	42.98	43.21	42.47	70.48	113.27
363.15	43.21	29.31	36.63	36.5	35.96	59.54	94.14
373.15	33.20	23.52	28.97	28.52	28.19	46.52	72.26
378.15	30.44	22.08	26.97	26.38	26.13	43.04	66.22
383.15	35.11	26.1	31.61	30.71	30.48	50.09	76.31

Table 3. *Cont.*

T (K)	Hamieh Thermal Model	Geometric	Cylindrical	Van Der Waals	Kiselev	Redlich–Kwong	Spherical
Adsorption of PMMA on Silica for θ=0.31							
388.15	**50.63**	**38.41**	**46.07**	**44.44**	**44.2**	**72.48**	**109.28**
393.15	40.82	32.01	38.03	36.4	36.29	59.37	88.54
398.15	34.59	27.92	32.83	31.17	31.15	50.84	74.96
403.15	29.88	24.86	28.9	27.21	27.26	44.38	64.64
408.15	24.15	20.61	23.64	22.04	22.15	35.94	51.66
413.15	19.32	17.21	19.5	18.01	18.14	29.37	41.65
423.15	16.27	15.72	17.26	15.57	15.8	25.39	34.89
433.15	27.30	24.3	25.49	22.26	22.8	36.31	47.82
443.15	**17.37**	**16.08**	**18.28**	**17.25**	**17.27**	**28.14**	**40.03**
453.15	12.73	12.76	14.1	12.99	13.08	21.19	29.29
463.15	9.74	10.79	11.48	10.27	10.42	16.75	22.36
473.15	9.17	9.30	10.39	10.04	9.59	16.38	22.16
Adsorption of PMMA on Silica for $\theta = 0.98$							
303.15	80.49	44.54	59.44	62.52	60.6	101.99	175.35
313.15	72.76	41.43	54.81	57.22	55.58	93.35	158.6
323.15	63.27	37.13	48.66	50.4	49.07	82.22	137.94
328.15	65.85	39.28	51.21	52.81	51.49	86.15	143.6
333.15	**70.99**	**43.04**	**55.83**	**57.32**	**55.96**	**93.51**	**154.82**
338.15	64.89	40.21	51.86	52.91	51.82	86.31	142.04
343.15	59.74	37.5	48.09	48.93	47.9	79.81	130.25
348.15	54.14	34.5	44.12	44.68	43.79	72.87	117.65
353.15	49.63	32.34	40.97	41.27	40.52	67.32	108.2
363.15	40.84	27.7	34.62	34.5	33.98	56.27	88.97
373.15	31.81	22.54	27.76	27.33	27.02	44.58	69.25
378.15	32.08	23.19	28.37	27.82	27.54	45.38	69.63
383.15	36.69	27.28	33.04	32.1	31.86	52.36	79.76
388.15	**53.25**	**40.64**	**48.75**	**47.02**	**46.77**	**76.68**	**115.61**
393.15	46.15	39.19	43.00	41.16	41.03	67.13	100.11
398.15	40.22	32.46	38.16	36.24	36.21	59.1	87.13
403.15	29.26	24.35	28.31	26.65	26.7	43.47	63.32
408.15	22.52	19.22	22.05	20.55	20.66	33.52	48.18
413.15	18.87	16.79	19.04	17.59	17.72	28.7	40.63
423.15	16.30	15.75	17.29	15.6	15.82	25.44	34.96
433.15	27.59	24.55	25.75	22.49	23.04	36.68	48.31
443.15	**15.59**	**14.42**	**16.41**	**15.48**	**15.5**	**25.25**	**35.92**
453.15	10.59	10.61	11.72	10.8	10.88	17.62	24.36
463.15	8.16	9.04	9.62	8.6	8.73	14.03	18.74
473.15	7.66	7.77	8.68	8.39	8.01	13.68	18.51
Adsorption of PMMA on Silica for $\theta = 1.0$							
303.15	75.92	42.01	56.07	58.97	57.16	96.2	165.4
313.15	67.65	38.52	50.96	53.21	51.68	86.8	147.47
323.15	58.85	34.54	45.27	46.89	45.65	76.4	128.33
328.15	61.70	36.8	47.98	49.48	48.24	80.71	134.54
333.15	**67.28**	**40.79**	**52.91**	**54.33**	**53.04**	**88.62**	**146.73**
338.15	61.50	38.11	49.15	50.15	49.12	81.8	134.63
343.15	56.07	35.19	45.14	45.93	44.96	74.92	122.27

Table 3. *Cont.*

| Adsorption of PMMA on Silica for $\theta=0.31$						
T (K)	Hamieh Thermal Model	Geometric	Cylindrical	Van Der Waals	Kiselev	Redlich–Kwong	Spherical
348.15	50.99	32.6	41.56	42.08	41.25	68.64	111.18
353.15	46.12	30.05	38.07	38.35	37.65	62.55	100.54
363.15	37.96	25.75	32.18	32.07	31.59	52.31	82.71
373.15	28.47	20.17	24.84	24.46	24.18	39.9	61.97
378.15	26.94	19.54	23.87	23.36	23.13	38.09	58.61
383.15	40.51	30.1	36.45	35.41	35.15	57.76	87.99
388.15	**55.89**	**42.66**	**51.17**	**49.35**	**49.09**	**80.5**	**121.36**
393.15	47.51	37.26	44.26	42.37	42.24	69.1	103.05
398.15	39.16	31.61	37.16	35.29	35.26	57.55	84.85
403.15	28.98	24.11	28.03	18.92	26.44	43.04	62.69
408.15	22.77	19.43	22.29	20.78	20.88	33.88	48.71
413.15	18.42	16.41	18.59	17.17	17.3	28	39.71
423.15	15.79	15.26	16.75	15.11	15.33	24.65	33.87
433.15	**25.97**	**24.38**	**25.61**	**22.38**	**22.93**	**36.5**	**48.15**
443.15	15.28	14.14	16.09	15.18	15.2	24.76	35.23
453.15	10.19	10.21	11.28	10.4	10.47	16.96	23.44
463.15	7.71	8.58	9.11	8.13	8.26	13.26	17.7
473.15	7.39	7.49	8.37	8.09	7.72	13.19	17.85
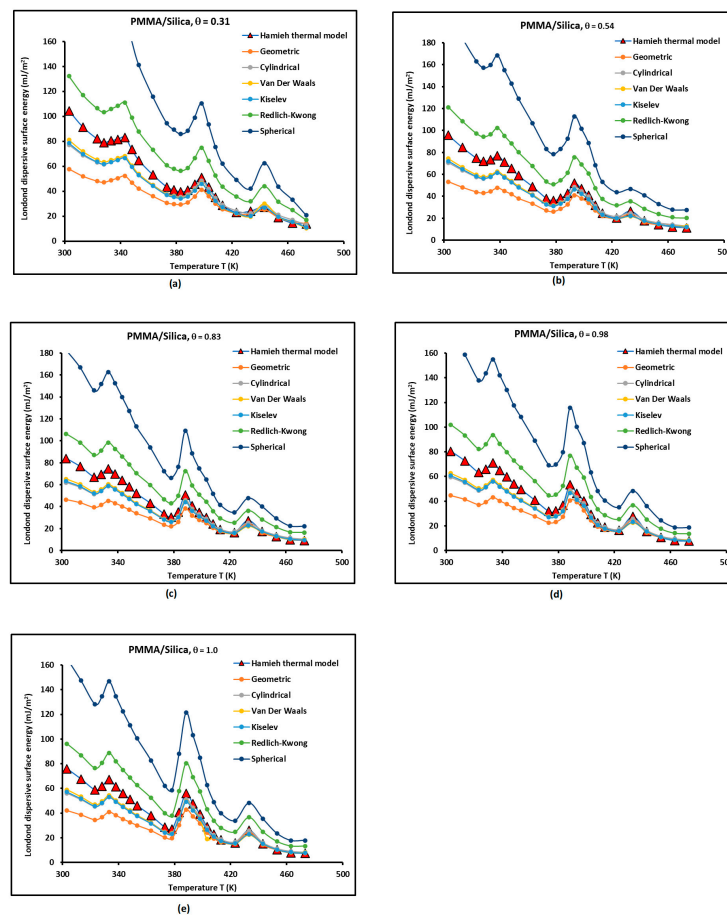
Figure 5. Variations of $\gamma_s^d\,(T)$ of PMMA adsorbed on silica particles as a function of the temperature at different recovery fractions from $\theta = 0.31$ to $\theta = 1.0$ using the various molecular models: (**a**) $\theta = 0.31$, (**b**) $\theta = 0.54$, (**c**) $\theta = 0.83$, (**d**) $\theta = 0.98$, and (**e**) $\theta = 1.0$.

- The London dispersive surface energy decreases when the recovery fraction fractions of PMMA adsorbed on silica increases whatever the used molecular model;
- The adsorption of PMMA on silica strongly affects the physicochemical properties of PMMA relative to its bulk phase. The transition temperatures observed in PMMA alone change with the recovery fraction;
- When approaching the monolayer of adsorption of PMMA on silica particles, there is a spontaneous decreasing evolution of the London dispersive surface energy from silica particles (Table 1) to PMMA in the bulk phase (Table 2), and when passing through the different recovery fractions from $\theta = 0.31$ to $\theta = 1.0$ (Table 3 and Figure 5), the behavior of the PMMA monolayer becomes closer to PMMA in its bulk phase.

The results given in Figure 5 and Table 3 give the various transition temperatures of PMMA adsorbed on silica particles at different recovery fractions. The obtained values are presented in Table S3 and Figure 6. It was observed that the beta-relaxation temperature linearly decreased from $T_\beta = 343.15$ K to stabilize at $T_\beta = 333.15$ K for $\theta = 0.83$, and the same value was observed for PMMA alone, whereas the glass transition decreased from $T_g = 398.15$ K to $T_g = 383.15$ K for $\theta = 0.83$, and then it increased to $T_g = 388.15$ K to reach the value $T_g = 383.15$ K for PMMA. However, the liquid–liquid transition temperature oscillated between $T_{l-l} = 443.15$ K and $T_{l-l} = 433.15$ K. Therefore, there is an important effect of the adsorption of PMMA on the London dispersive energy of the PMMA/silica systems and the transition temperatures. Those results were confirmed for all molecular models.
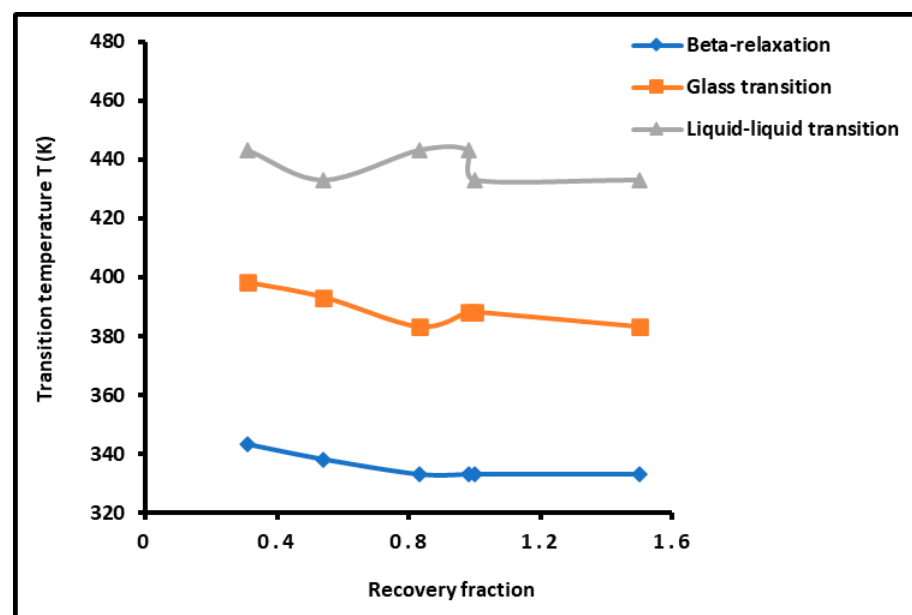

Figure 6. Evolution of the transition temperatures of PMMA adsorbed on silica particles as a function of the recovery fraction PMMA/silica.
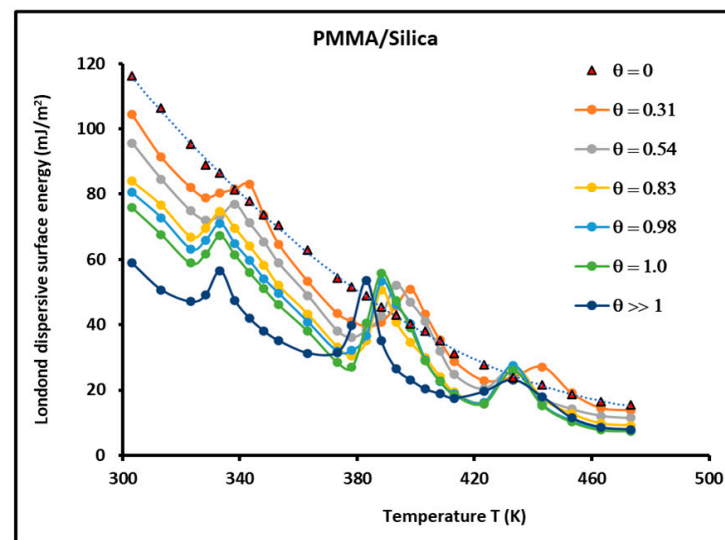
Furthermore, the London dispersive surface energy of the PMMA/silica composites at the different transition temperatures strongly varied as a function of the recovery fraction. These variations of γ_s^d are clearly shown in Table 4. A decrease in the London dispersive energy was observed before reaching the monolayer in the cases of beta-relaxation and liquid–liquid transitions, whereas a small change was found in the case of the glass transition. Table 4 also shows that after the monolayer, the different values of γ_s^d approached those of PMMA.

In fact, the above observations can be generalized for all temperatures and recovery fractions, as shown in Figure 7. The curves plotted in Figure 7a show the shift of the maxima of the various transition temperatures when the recovery fraction of PMMA/silica varied. Furthermore, the variations of $\gamma_s^d(\theta)$ were perfectly linear for all temperatures far from the transition temperatures, as shown in Figure 7b. The results show a decrease in
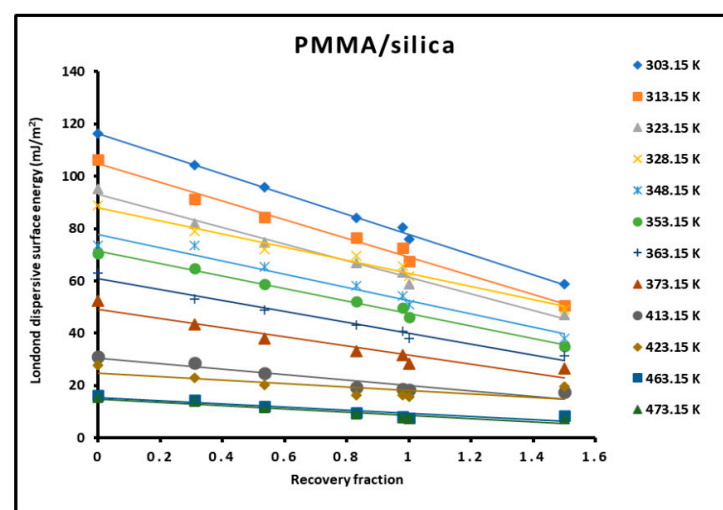
the London dispersive surface energy of PMMA/silica when the temperature and/or the recovery increased. The different equations of $\gamma_s^d(\theta)$ are given in Table 5. The linearity is shown by the good linear regression coefficients shown in Table 5.

Table 4. Values of the London dispersive surface energy γ_s^d (mJ/m^2) of PMMA/silica composites at the transition temperatures as a function of the recovery fraction.

Recovery Fraction of PMMA/Silica θ	Beta-Relaxation Temperature T_β	Glass Transition Temperature T_g	Liquid–Liquid Temperature T_{l-l}
0.31	83.10	50.97	27.13
0.54	76.92	52.06	26.55
0.83	74.62	50.63	17.37
0.98	70.99	53.26	15.59
1.0	67.28	55.89	25.97
PMMA	56.62	53.54	23.16

(a)

(b)

Figure 7. Variations of the London dispersive energy of silica and PMMA adsorbed on silica particles as a function of the temperature and the recovery fraction PMMA/Silica. (**a**) $\gamma_s^d(T)$ and (**b**) $\gamma_s^d(\theta)$.

Table 5. Equation of London dispersive surface energy $\gamma_s^d(\theta)$ of PMMA/silica composites at different temperatures far from the transition temperatures with the linear regression coefficients and the values of $(-d\gamma_s^d/d\theta)$ and $\gamma_s^d(0)$.

T (K)	Equation of $\gamma_s^d(\theta)$	R^2	$-d\gamma_s^d/d\theta$	$\gamma_s^d(0)$
303.15	$\gamma_s^d(\theta) = -38.63\,\theta + 116.32$	0.994	38.63	116.32
313.15	$\gamma_s^d(\theta) = -34.92\,\theta + 104.49$	0.9779	34.92	104.49
323.15	$\gamma_s^d(\theta) = -33.44\,\theta + 93.92$	0.985	33.44	93.92
328.15	$\gamma_s^d(\theta) = -23.85\,\theta + 87.36$	0.9569	23.85	87.36
348.15	$\gamma_s^d(\theta) = -23.40\,\theta + 76.95$	0.9293	23.40	76.95
353.15	$\gamma_s^d(\theta) = -23.26\,\theta + 71.15$	0.9865	23.26	71.15
363.15	$\gamma_s^d(\theta) = -22.75\,\theta + 61.70$	0.9836	22.75	61.70
373.15	$\gamma_s^d(\theta) = -23.19\,\theta + 52.36$	0.9658	23.19	52.36
413.15	$\gamma_s^d(\theta) = -13.59\,\theta + 31.82$	0.9765	13.59	31.82
423.15	$\gamma_s^d(\theta) = -11.84\,\theta + 27.13$	0.9751	11.84	27.13
463.15	$\gamma_s^d(\theta) = -8.69\,\theta + 16.72$	0.9918	8.69	16.72
473.15	$\gamma_s^d(\theta) = -8.27\,\theta + 15.87$	0.9904	8.27	15.87

Table 5 led to the following thermodynamic relations of $(-\frac{d\gamma_s^d}{d\theta}(T))$ and $\gamma_s^d(T, 0)$ as a function of the temperature as follows:

$$\begin{cases} -\frac{d\gamma_s^d}{d\theta}(T) = 8 \times 10^{-4}\,T^2 - 0.759\,T + 197.04; \ R^2 = 0.9453 \\ \gamma_s^d(T,0) = 2.8 \times 10^{-3}\,T^2 - 2.77\,T + 696.64; \ R^2 = 0.9972 \end{cases} \tag{6}$$

Relation 6 then gives a universal equation of the following form:

$$\gamma_s^d(T, \theta) = \frac{d\gamma_s^d}{d\theta}(T)\,\theta + \gamma_s^d(T, 0) \tag{7}$$

Equation (7) is the general form of the dependence of the London dispersive surface energy of the PMMA/silica composites on the temperature and the recovery fraction θ. The expression of $\gamma_s^d(T, 0)$ given in Relation 3 gave the same equation as that obtained with the silica particles (for $\theta = 0$). The obtained linearity of γ_s^d as a function of θ is not realized with the temperature. Indeed, the second-degree equation of $(-\frac{d\gamma_s^d}{d\theta}(T))$ and $\gamma_s^d(T, 0)$ versus the temperature gave a non-linearity dependence of $\gamma_s^d(T)$.

The Equation (7) can be written for a constant temperature as follows:

$$\theta \frac{d\gamma_s^d}{d\theta} - \gamma_s^d(\theta) + \gamma_s^d(0) = 0 \tag{8}$$

Equation (8) is then an ordinary first-order differential equation of $\gamma_s^d(\theta)$. It can be easily integrated. $\gamma_s^d(\theta)$ is, therefore, given at any temperature *T* by Equation (13) as follows:

$$\gamma_s^d(\theta) = \left(\gamma_s^d(\theta = 1) - \gamma_s^d(\theta = 0)\right)\theta + \gamma_s^d(0) \tag{9}$$

where $\gamma_s^d(0)$ and $\gamma_s^d(1)$ represent the respective values of the London dispersive energy of silica ($\theta = 0$) and PMMA/silica for $\theta = 1$ at a fixed temperature *T*.

The results obtained from the integrated theoretical Equation (9) can be compared to the experimental results given in Table 5. As examples, we show in Table 6 the theoretical results at three temperatures of 303.15 K, 363.15 K, and 473.15 K.

The comparison between the theoretical results given in Table 6 with the experimental results given in Table 5 show excellent agreement. The difference between the two results did not exceed 2%.

Table 6. Theoretical results of $\gamma_s^d(\theta)$ of PMMA/silica composites at three temperatures with the values of $(-d\gamma_s^d/d\theta)$ and $\gamma_s^d(0)$.

T (K)	Equation of $\gamma_s^d(\theta)$	$-d\gamma_s^d/d\theta$	$\gamma_s^d(0)$
303.15	$\gamma_s^d(\theta) = -40.37\,\theta + 116.29$	40.37	116.29
363.15	$\gamma_s^d(\theta) = -37.96\,\theta + 62.86$	37.96	62.86
473.15	$\gamma_s^d(\theta) = -8.08\,\theta + 15.47$	8.08	15.47

3.3. Lewis's Acid-Base Polar Surface Energies of PMMA/Silica

Van Oss et al.'s method [85] was used to determine the Lewis acid γ_s^+ and base γ_s^- surface energies of PMMA/silica knowing the Lewis acid γ_l^+ and base γ_l^- surface energies of the used solvents. Van Oss et al. [85] used two monopolar solvents, namely, ethyl acetate (*EA*) and dichloromethane (*DCM*), which are usually characterized by

$$\begin{cases} \gamma_{DCM}^+ = 5.2 \text{ mJ/m}^2 \,,\ \gamma_{DCM}^- = 0 \\ \gamma_{EA}^+ = 0 \,,\ \gamma_{EA}^- = 19.2 \text{ mJ/m}^2 \end{cases} \tag{10}$$

In previous studies [53,54], the polar-free energy $\Delta G_a^{sp}(T)$ of the different PMMA/silica composites was determined as a function of the temperature with various recovery fractions. Knowing that, $\Delta G_a^{sp}(T)$ can be expressed as follows:

$$\Delta G_a^{sp}(T) = 2\mathcal{N}a\left(\sqrt{\gamma_l^-\gamma_s^+} + \sqrt{\gamma_l^+\gamma_s^-}\right) \tag{11}$$

The Lewis acid and base surface energies of the various PMMA/silica composites were determined with the help of the following equations:

$$\begin{cases} \gamma_s^+ = \dfrac{\left[\Delta G_a^{sp}(T)(EA)\right]^2}{4\mathcal{N}^2[a(EA)]^2\gamma_{EA}^-} \\ \gamma_s^- = \dfrac{\left[\Delta G_a^{sp}(T)(DCM)\right]^2}{4\mathcal{N}^2[a(DCM)]^2\gamma_{DCM}^+} \end{cases} \tag{12}$$

using the values of the surface area of polar molecules obtained from the Hamieh thermal model. The obtained values of $\Delta G_a^{sp}(T)$ of EA and DCM adsorbed on the different solid surfaces are given in Tables S4 and S5. The polar (or acid-base) surface energy γ_s^{AB} and the total surface energy of different PMMA/silica composites were obtained in Equation (13).

$$\begin{cases} \gamma_s^{AB} = 2\sqrt{\gamma_s^+\gamma_s^-} \\ \gamma_s^{tot.} = \gamma_s^d + \gamma_s^{AB} \end{cases} \tag{13}$$

The results are presented in Table S6 and Figure 8. All surface energy parameters of the various PMMA/silica varied as a function of the temperature, as shown in Figure 8.
Several conclusions can be deduced as follows:

- All curves of the acid-base polar surface energies decreased against the temperature, except at the transition temperature where higher values of these parameters were observed for the different recovery fractions.
- The acid polar surface energy of silica did not present any appreciated variation when the recovery fraction of PMMA increased. Globally, the acidity of silica particles is not very affected by the adsorbed amount of PMMA.
- An important change in the value of the base polar surface energy $\gamma_s^-(T)$ was observed when the recovery fraction of PMMA varied. It seems that a maximum of $\gamma_s^-(T)$ was obtained in the case of a monolayer ($\theta = 1.0$) of PMMA adsorbed on silica particles, and the acid-base polar surface energy γ_s^{AB} was the highest in this later case. For this value of $\theta = 1.0$, a maximum of $\gamma_s^{tot.}(T)$ was also observed. In the case of the monolayer of adsorption of PMMA on silica, it can be deduced that the polar surface energy was higher than those of silica and PMMA taken separately, and it

approximately approached the summation of these two extreme cases of $\theta = 0$ (*Silica*) and PMMA in the bulk phase.

- Figure 8 shows all curves of the Lewis acid-base surface energies as a function of the temperature and gave similar variations as those of $\gamma_s^d(T)$. The behavior of these Lewis surface parameters showed an increase before every transition temperature until reaching their maximum values at the transition temperature directly followed by a decrease in the Lewis surface energies. These variations of neighboring transition temperatures are due to the fluctuations and relaxation of the chain groups of PMMA as a function of the temperature.
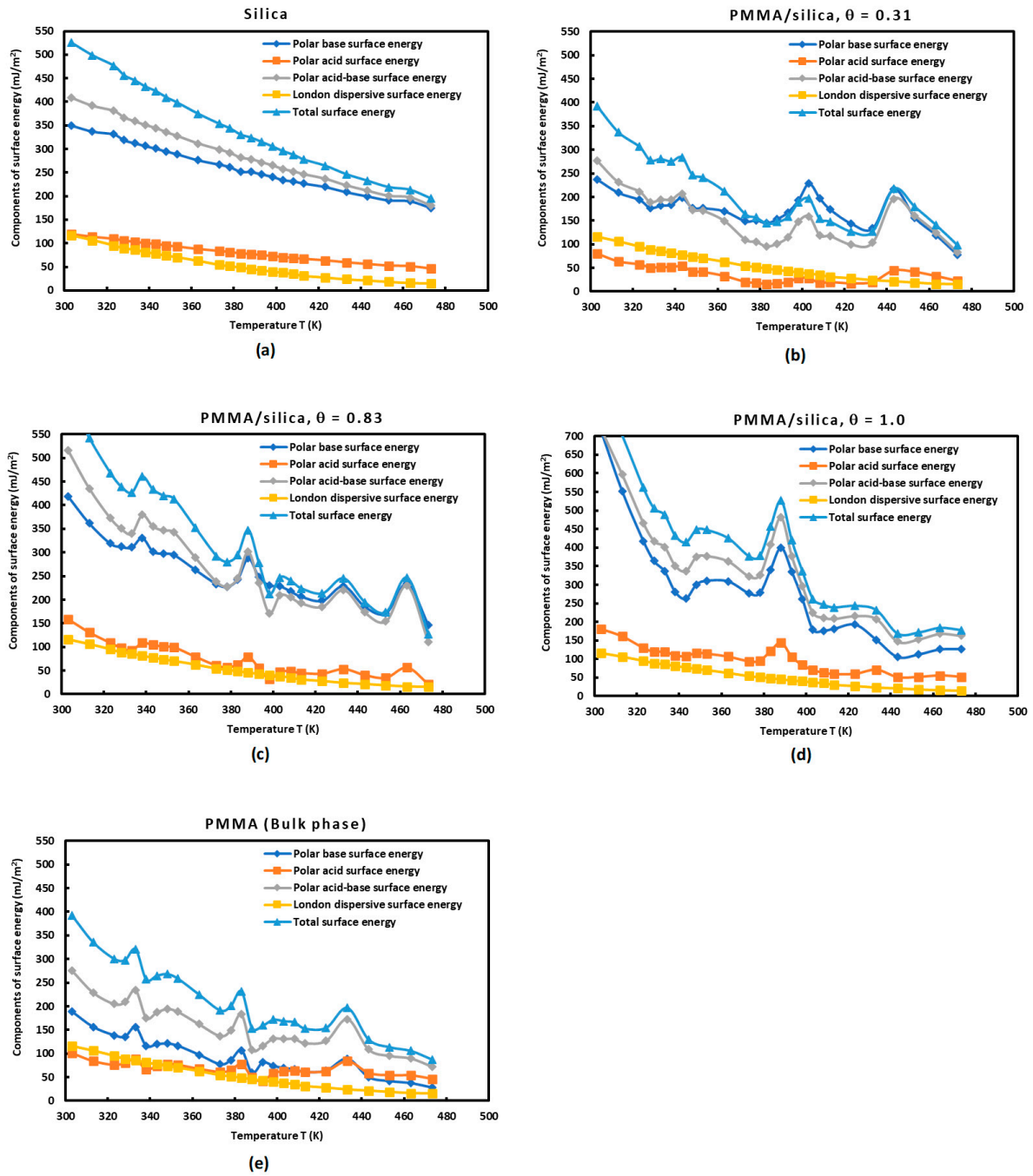
Figure 8. Variations of $\gamma_s^+(T)$, $\gamma_s^-(T)$, $\gamma_s^{AB}(T)$, $\gamma_s^{tot.}(T)$, and $\gamma_s^d(T)$ of silica particles and PMMA adsorbed on silica as a function of the temperature at different recovery fractions. (**a**) $\theta = 0$ (*silica case*), (**b**) $\theta = 0.31$, (**c**) $\theta = 0.83$, (**d**) $\theta = 1.0$, and (**e**) $\theta \gg 1$ (*PMMA case*).

4. Conclusions

The adsorption of PMMA on silica particles at different recovery fractions was studied as a function of the temperature using inverse gas chromatography (IGC) at infinite dilution. The IGC technique gave the experimental values of $RTlnV_n$ of n-alkanes adsorbed on the different PMMA/silica composites. Several molecular models were used and compared to the recent Hamieh thermal model to determine the variations of the London dispersive surface energy of solid particles as a function of the temperature and the recovery fraction of PMMA adsorbed on silica. The determination of $\gamma_s^d(T)$ of silica particles using the thermal model showed parabolic variations with an excellent regression coefficient approaching 1.000. The other molecular models gave the same type of variations of $\gamma_s^d(T)$ but with important deviation from the accurate thermal model, taking into account the effect of the temperature on the surface area of organic molecules. The curves of $\gamma_s^d(T)$ of the PMMA/silica systems confirmed the presence of three maxima, characterizing the three transition temperatures of the beta-relaxation, the glass transition, and the liquid–liquid transition. An important effect of the recovery fraction of PMMA on the values of the transition temperatures was highlighted in this study.

A universal equation of $\gamma_s^d(T, \theta)$ of the various PMMA/silica composites was given as a function of the two variables, the temperature T, and the recovery fraction θ. The determination of the couple (T, θ) led to obtaining the value of γ_s^d and the full thermodynamic determination of the PMMA/silica system.

The Lewis acid γ_s^+ and base γ_s^- polar surface energies of PMMA/silica composites were determined using the thermal model as a function of the temperature and the recovery fraction. The polar acid-base surface energy γ_s^{AB} and the total surface energy of the different composites were then deduced. It was shown that γ_s^+ of silica was not very affected by the adsorption of PMMA on silica, whereas γ_s^- presented large variations when the recovery fraction varied. A maximum of basic and total polar surface energies was reached in the case of the monolayer of PMMA. The total polar surface energy of PMMA/silica for a monolayer ($\theta = 1.0$) was proved to be approximately equivalent, out of the transition temperatures, to the summation of those obtained with silica and PMMA solid surfaces.

References

1. Papadopoulou, S.K.; Panayiotou, C. Assessment of the thermodynamic properties of poly(2,2,2-trifluoroethyl methacrylate) by inverse gas chromatography. *J. Chromatogr. A* **2014**, *1324*, 207–214. [CrossRef] [PubMed]
2. Voelkel, A.; Strzemiecka, B.; Adamska, K.; Milczewska, K. Inverse gas chromatography as a source of physiochemical data. *J. Chromatogr. A* **2009**, *1216*, 1551. [CrossRef] [PubMed]
3. Al-Saigh, Z.Y.; Munk, P. Study of polymer-polymer interaction coefficients in polymer blends using inverse gas chromatography. *Macromolecules* **1984**, *17*, 803. [CrossRef]
4. Dritsas, G.S.; Karatasos, K.; Panayiotou, C. Investigation of thermodynamic properties of hyperbranched aliphatic polyesters by inverse gas chromatography. *J. Chromatogr. A* **2009**, *1216*, 8979. [CrossRef]
5. Papadopoulou, S.K.; Karapanagiotis, I.; Zuburtikudis, I.; Panayiotou, C. Thermodynamic characterization of poly(2,2,3,3,3-pentafluoropropyl methacrylate). *J. Polym. Sci. B Polym. Phys.* **2010**, *48*, 1826. [CrossRef]
6. Papadopoulou, S.K.; Panayiotou, C. Thermodynamic characterization of poly(1,1,1,3,3,3-hexafluoroisopropyl methacrylate) by inverse gas chromatography. *J. Chromatogr. A* **2012**, *1229*, 230. [CrossRef]
7. Coimbra, P.; Coelho, M.S.N.; Gamelas, J.A.F. Surface characterization of polysaccharide scaffolds by inverse gas chromatography regarding application in tissue engineering. *Surf. Interface Anal.* **2019**, *51*, 1070–1077. [CrossRef]
8. Kołodziejek, J.; Voelkel, A.; Heberger, K. Characterization of hybrid materials by means of inverse gas chromatography and chemometrics. *J. Pharm. Sci.* **2013**, *102*, 1524. [CrossRef]
9. Heydar, K.; Nazifi, M.; Sharifi, A.; Mirzaei, M.; Gharavi, H.; Ahmadi, S. Determination of Activity Coefficients at Infinite Dilution of Solutes in New Dicationic Ionic Liquids Based on Morpholine Using Gas–Liquid Chromatography. *Chromatographia* **2013**, *76*, 165. [CrossRef]
10. Doman'ska, U.; Lukoshko, E.V. Measurements of activity coefficients at infinite dilution for organic solutes and water in the ionic liquid 1-butyl-1-methylpyrrolidinium tricyanomethanide. *J. Chem. Therm.* **2013**, *66*, 144. [CrossRef]
11. Yoo, B.; Afzal, W.; Prausnitz, J.M. Solubility parameters for nine ionic liquids. *Ind. Eng. Chem. Res.* **2012**, *51*, 9913. [CrossRef]
12. Lazar, P.; Karlický, F.; Jurečka, P.; Kocman, M.; Otyepková, E.; Šafářová, K.; Otyepka, M. Adsorption of small organic molecules on graphene. *J. Am. Chem. Soc.* **2013**, *135*, 6372–6377. [CrossRef] [PubMed]
13. Belgacem, M.N.; Czeremuszkin, G.; Sapieha, S.; Gandini, A. Surface by XPS characterization and inverse gas of cellulose fibres chromatography. *Cellulose* **1995**, *2*, 145–157. [CrossRef]
14. Papadopoulou, S.K.; Tsioptsias, C.; Pavlou, A.; Kaderides, K.; Sotiriou, S.; Panayiotou, C. Superhydrophobic surfaces from hydrophobic or hydrophilic polymers via nanophase separation or electrospinning/electrospraying. *Colloids Surf. A* **2011**, *387*, 71–78. [CrossRef]
15. Ryan, H.M.; Douglas, J.G.; Rupert, W. Inverse Gas Chromatography for Determining the Dispersive Surface Free Energy and Acid-Base Interactions of Sheet Molding Compound-Part II 14 Ligno-Cellulosic Fiber Types for Possible Composite Reinforcement. *J. Appl. Polym. Sci.* **2008**, *110*, 3880–3888.
16. Jacob, P.N.; Berg, J.C. Acid-base surface energy characterization of microcrystalline cellulose and two wood pulp fiber types using inverse gas chromatography. *Langmuir* **1994**, *10*, 3086–3093. [CrossRef]
17. Carvalho, M.G.; Santos, J.M.R.C.A.; Martins, A.A.; Figueiredo, M.M. The Effects of Beating, Web Forming and Sizing on the Surface Energy of *Eucalyptus globulus* Kraft Fibres Evaluated by Inverse Gas Chromatography. *Cellulose* **2005**, *12*, 371–383. [CrossRef]
18. Chtourou, H.; Riedl, B.; Kokta, B.V. Surface characterizations of modified polyethylene pulp and wood pulps fibers using XPS and inverse gas chromatography. *J. Adhesion Sci. Technol.* **1995**, *9*, 551–574. [CrossRef]
19. Dorris, G.M.; Gray, D.G. Adsorption of *n*-alkanes at zero surface coverage on cellulose paper and wood fibers. *J. Colloid Interface Sci.* **1980**, *77*, 353–362. [CrossRef]
20. Donnet, J.B.; Park, S.J.; Balard, H. Evaluation of specific interactions of solid surfaces by inverse gas chromatography. *Chromatographia* **1991**, *31*, 434–440. [CrossRef]
21. Donnet, J.B.; Custodéro, E.; Wang, T.K.; Hennebert, G. Energy site distribution of carbon black surfaces by inverse gas chromatography at finite concentration conditions. *Carbon* **2002**, *40*, 163–167. [CrossRef]
22. Gamble, J.F.; Davé, R.N.; Kiang, S.; Leane, M.M.; Tobyn, M.; Wang, S.S.Y. Investigating the applicability of inverse gas chromatography to binary powdered systems: An application of surface heterogeneity profiles to understanding preferential probe-surface interactions. *Int. J. Pharm.* **2013**, *445*, 39–46. [CrossRef] [PubMed]
23. Balard, H.; Maafa, D.; Santini, A.; Donnet, J.B. Study by inverse gas chromatography of the surface properties of milled graphites. *J. Chromatogr. A* **2008**, *1198–1199*, 173–180. [CrossRef]
24. Bogillo, V.I.; Shkilev, V.P.; Voelkel, A. Determination of surface free energy components for heterogeneous solids by means of inverse gas chromatography at finite concentrations. *J. Mater. Chem.* **1998**, *8*, 1953–1961. [CrossRef]
25. Das, S.C.; Zhou, Q.; Morton, D.A.V.; Larson, I.; Stewart, P.J. Use of surface energy distributions by inverse gas chromatography to understand mechanofusion processing and functionality of lactose coated with magnesium stearate. *Eur. J. Pharm. Sci.* **2011**, *43*, 325–333. [CrossRef]
26. Das, S.C.; Stewart, P.J. Characterising surface energy of pharmaceutical powders by inverse gas chromatography at finite dilution. *J. Pharm. Pharmacol.* **2012**, *64*, 1337–1348. [CrossRef]

27. Bai, W.; Pakdel, E.; Li, Q.; Wang, J.; Tang, W.; Tang, B.; Wang, X. Inverse gas chromatography (IGC) for studying the cellulosic materials surface characteristics: A mini review. *Cellulose* **2023**, *30*, 3379–3396. [CrossRef]

28. Dong, S.; Brendlé, M.; Donnet, J.B. Study of solid surface polarity by inverse gas chromatography at infinite dilution. *Chromatographia* **1989**, *28*, 469–472. [CrossRef]

29. Feeley, J.C.; York, P.; Sumby, B.S.; Dicks, H. Determination of surface properties and flow characteristics of salbutamol sulphate, before and after micronisation. *Int. J. Pharm.* **1998**, *172*, 89–96. [CrossRef]

30. Gamble, J.F.; Leane, M.; Olusanmi, D.; Tobyn, M.; Supuk, E.; Khoo, J.; Naderi, M. Surface energy analysis as a tool to probe the surface energy characteristics of micronized materials—A comparison with inverse gas chromatography. *Int. J. Pharm.* **2012**, *422*, 238–244. [CrossRef]

31. Newell, H.E.; Buckton, G.; Butler, D.A.; Thielmann, F.; Williams, D.R. The use of inverse gas chromatography to measure the surface energy of crystalline, amorphous, and recently milled lactose. *Pharm. Res.* **2001**, *18*, 662–666. [CrossRef] [PubMed]

32. Newell, H.E.; Buckton, G. Inverse gas chromatography: Investigating whether the technique preferentially probes high energy sites for mixtures of crystalline and amorphous lactose. *Pharm. Res.* **2004**, *21*, 1440–1444. [CrossRef]

33. Kołodziejek, J.; Głowka, E.; Hyla, K.; Voelkel, A.; Lulek, J.; Milczewska, K. Relationship between surface properties determined by inverse gas chromatography and ibuprofen release from hybrid materials based on fumed silica. *Int. J. Pharm.* **2013**, *441*, 441–448. [CrossRef] [PubMed]

34. Ho, R.; Wilson, D.A.; Heng, J.Y.Y. Crystal habits and the variation in surface energy heterogeneity. *Cryst. Growth Des.* **2009**, *9*, 4907–4911. [CrossRef]

35. Ho, R.; Hinder, S.J.; Watts, J.F.; Dilworth, S.E.; Williams, D.R.; Heng, J.Y.Y. Determination of surface heterogeneity of D-mannitol by sessile drop contact angle and finite concentration inverse gas chromatography. *Int. J. Pharm.* **2010**, *387*, 79–86. [CrossRef]

36. Ho, R.; Naderi, M.; Heng, J.Y.Y.; Williams, D.R.; Thielmann, F.; Bouza, P.; Keith, A.R.; Thiele, G.; Burnett, D.J. Effect of milling on particle shape and surface energy heterogeneity of needle-shaped crystals. *Pharm. Res.* **2012**, *29*, 2806–2816. [CrossRef] [PubMed]

37. Sesigur, F.; Sakar, D.; Yazici, O.; Cakar, F.; Cankurtaran, O.; Karaman, F. Dispersive Surface Energy and Acid-Base Parameters of Tosylate Functionalized Poly(ethylene glycol) via Inverse Gas Chromatography. *J. Chem.* **2014**, *2014*, 402325. [CrossRef]

38. Calvet, R.; Del Confetto, S.; Balard, H.; Brendlé, E.; Donnet, J.B. Study of the interaction polybutadiene/fillers using inverse gas chromatography. *J. Chromatogr. A* **2012**, *1253*, 164–170. [CrossRef]

39. Papadopoulou, S.K.; Dritsas, G.; Karapanagiotis, I.; Zuburtikudis, I.; Panayiotou, C. Surface characterization of poly(2,2,3,3,3-pentafluoropropyl methacrylate) by inverse gas chromatography and contact angle measurements. *Eur. Polym. J.* **2010**, *46*, 202–208. [CrossRef]

40. Dritsas, G.S.; Karatasos, K.; Panayiotou, C. Investigation of thermodynamic properties of hyperbranched poly(ester amide) by inverse gas chromatography. *J. Polym. Sci. Polym. Phys.* **2008**, *46*, 2166–2172. [CrossRef]

41. Ishihara, M.; Watanabe, T.; Hirata, T.; Sasaki, T. Melt adsorption of poly(*tert*-butyl methacrylate) and poly(ethyl methacrylate) on silica studied with chip nanocalorimetry. *Polym. J.* **2024**, *276*, 517–527. [CrossRef]

42. Napolitano, S. Irreversible adsorption of polymer melts and nanoconfinement effects. *Soft Matter* **2020**, *16*, 5348–5365. [CrossRef]

43. Gawek, M.; Omar, H.; Szymoniak, P.; Schönhals, A. Growth kinetics of the adsorbed layer of poly(2-vinylpyridine)—An indirect observation of desorption of polymers from substrates. *Soft Matter* **2023**, *19*, 3975–3982. [CrossRef]

44. Zuo, B.; Zhou, H.; Davis, M.J.; Wang, X.; Priestley, R.D. Effect of local chain conformation in adsorbed nanolayers on confined polymer molecular mobility. *Phys. Rev. Lett.* **2019**, *122*, 217801. [CrossRef] [PubMed]

45. Huang, J.; Zhou, J.; Liu, M. Interphase in polymer nanocomposites. *ACS Au* **2022**, *2*, 280–291. [CrossRef]

46. Tian, H.; Bi, C.; Li, Z.; Wang, C.; Zuo, B. Metastable polymer adsorption dictates the dynamical gradients at interfaces. *Macromolecules* **2023**, *56*, 4346–4353. [CrossRef]

47. Wang, N.; Wu, X.; Liu, C.S. Opposite Effects of SiO$_2$ Nanoparticles on the Local α and Larger-Scale α' Segmental Relaxation Dynamics of PMMA Nanocomposites. *Polymers* **2019**, *11*, 979. [CrossRef] [PubMed]

48. Ma, M.; Cui, W.; Guo, Y.; Yu, W. Adsorption-desorption effect on physical aging in PMMA-silica nanocomposites. *Polymer* **2022**, *255*, 125124. [CrossRef]

49. Cui, W.; You, W.; Sun, Z.; Yu, W. Decoupled polymer dynamics in weakly attractive poly(methyl methacrylate)/silica nanocomposites. *Macromolecules* **2021**, *54*, 5484–5497. [CrossRef]

50. Boucher, V.M.; Cangialosi, D.; Alegría, A.; Colmenero, J. Enthalpy recovery of PMMA/silica nanocomposites. *Macromolecules* **2010**, *43*, 7594–7603. [CrossRef]

51. Huang, C.-C.; Liu, C.-Y. Peculiar α-β relaxations of Syndiotactic-Poly(methyl methacrylate). *Polymer* **2021**, *225*, 123760. [CrossRef]

52. Kawaguchi, D.; Sasahara, K.; Inutsuka, M.; Abe, T.; Yamamoto, S.; Tanaka, K. Absolute local conformation of poly(methyl methacrylate) chains adsorbed on a quartz surface. *J. Chem. Phys.* **2023**, *159*, 244902. [CrossRef] [PubMed]

53. Hamieh, T.; Rezzaki, M.; Schultz, J. Study of the transition temperatures and acid-base properties of poly (methyl methacrylate) adsorbed on alumina and silica, by using inverse gas chromatography technique. *Colloids Surf. A Physicochem. Eng. Asp.* **2001**, *189*, 279–291. [CrossRef]

54. Hamieh, T.; Schultz, J. New approach to characterise physicochemical properties of solid substrates by inverse gas chromatography at infinite dilution. I. II. And III. *J. Chromatogr. A* **2002**, *969*, 17–47. [CrossRef] [PubMed]

55. Hamieh, T. Temperature Dependence of the Polar and Lewis Acid-Base Properties of Poly Methyl Methacrylate Adsorbed on Silica via Inverse Gas Chromatography. *Molecules* **2024**, *29*, 1688. [CrossRef]

56. Fowkes, F.M. Attractive forces at interfaces. *Ind. Eng. Chem.* **1964**, *56*, 40–52. [CrossRef]
57. Fowkes, F.M. Determination of interfacial tensions, contact angles, and dispersion forces in surfaces by assuming additivity of intermolecular interactions in surfaces. *J. Phys. Chem.* **1962**, *66*, 382. [CrossRef]
58. Fowkes, F.M. Additivity of intermolecular forces at interfaces. *J. Phys. Chem.* **1963**, *67*, 2538–2541. [CrossRef]
59. Hamieh, T. Study of the temperature effect on the surface area of model organic molecules, the dispersive surface energy and the surface properties of solids by inverse gas chromatography. *J. Chromatogr. A* **2020**, *1627*, 461372. [CrossRef]
60. Hamieh, T.; Ahmad, A.A.; Roques-Carmes, T.; Toufaily, J. New approach to determine the surface and interface thermodynamic properties of H-β-zeolite/rhodium catalysts by inverse gas chromatography at infinite dilution. *Sci. Rep.* **2020**, *10*, 20894. [CrossRef]
61. Hamieh, T. New methodology to study the dispersive component of the surface energy and acid-base properties of silica particles by inverse gas chromatography at infinite dilution. *J. Chromatogr. Sci.* **2022**, *60*, 126–142. [CrossRef] [PubMed]
62. Papirer, E.; Brendlé, E.; Ozil, F.; Balard, H. Comparison of the surface properties of graphite, carbon black and fullerene samples, measured by inverse gas chromatography. *Carbon* **1999**, *37*, 1265–1274. [CrossRef]
63. Chung, D.L. *Carbon Fiber Composites*; Butterworth-Heinemann: Boston, MA, USA, 1994; pp. 3–65. [CrossRef]
64. Donnet, J.B.; Bansal, R.C. *Carbon Fibers*, 2nd ed.; Marcel Dekker: New York, NY, USA, 1990; 584p. [CrossRef]
65. Friedlander, H.N.; Peebles, L.H., Jr.; Brandrup, J.; Kirby, J.R. On the chromophore of polyacrylonitrile. VI. Mechanism of color formation in polyacrylonitrile. *Macromolecules* **1968**, *1*, 79–86. [CrossRef]
66. Huang, X. Fabrication and Properties of Carbon Fibers. *Materials* **2009**, *2*, 2369–2403. [CrossRef]
67. Qiao, Z.; Ding, C. Recent progress in carbon fibers for boosting electrocatalytic energy conversion. *Ionics* **2022**, *28*, 5259–5273. [CrossRef]
68. Hamieh, T. Surface acid-base properties of carbon fibres. *Adv. Powder Technol.* **1997**, *8*, 279–289. [CrossRef]
69. Le Vu, H.; Nguyen, S.H.; Dang, K.Q.; Pham, C.V.; Le, H.T. The Effect of Oxidation Temperature on Activating Commercial Viscose Rayon-Based Carbon Fibers to Make the Activated Carbon Fibers (ACFs). *Mater. Sci. Forum* **2020**, *985*, 171–176. [CrossRef]
70. Liu, Y.; Gu, Y.; Wang, S.; Li, M. Optimization for testing conditions of inverse gas chromatography and surface energies of various carbon fiber bundles. *Carbon Lett.* **2023**, *33*, 909–920. [CrossRef]
71. Pal, A.; Kondor, A.; Mitra, S.; Thua, K.; Harish, S.; Saha, B.B. On surface energy and acid-base properties of highly porous parent and surface treated activated carbons using inverse gas chromatography. *J. Ind. Eng. Chem.* **2019**, *69*, 432–443. [CrossRef]
72. Hamieh, T. New Physicochemical Methodology for the Determination of the Surface Thermodynamic Properties of Solid Particles. *AppliedChem* **2023**, *3*, 229–255. [CrossRef]
73. Sawyer, D.T.; Brookman, D.J. Thermodynamically based gas chromatographic retention index for organic molecules using salt-modified aluminas and porous silica beads. *Anal. Chem.* **1968**, *40*, 1847–1850. [CrossRef]
74. Saint-Flour, C.; Papirer, E. Gas-solid chromatography. A method of measuring surface free energy characteristics of short carbon fibers. 1. Through adsorption isotherms. *Ind. Eng. Chem. Prod. Res. Dev.* **1982**, *21*, 337–341. [CrossRef]
75. Saint-Flour, C.; Papirer, E. Gas-solid chromatography: Method of measuring surface free energy characteristics of short fibers. 2. Through retention volumes measured near zero surface coverage. *Ind. Eng. Chem. Prod. Res. Dev.* **1982**, *21*, 666–669. [CrossRef]
76. Seulbee, L.; Lee, J.-H.; Kim, Y.-H.; Mahajan, R.L.; Park, S.-J. Surface energetics of graphene oxide and reduced graphene oxide determined by inverse gas chromatographic technique at infinite dilution at room temperature. *J. Colloid Interface Sci.* **2022**, *628*, 758–768.
77. Brendlé, E.; Papirer, E. A new topological index for molecular probes used in inverse gas chromatography for the surface nanorugosity evaluation, 2. Application for the Evaluation of the Solid Surface Specific Interaction Potential. *J. Colloid Interface Sci.* **1997**, *194*, 217–224. [CrossRef] [PubMed]
78. Brendlé, E.; Papirer, E. A new topological index for molecular probes used in inverse gas chromatography for the surface nanorugosity evaluation, 1. Method of Evaluation. *J. Colloid Interface Sci.* **1997**, *194*, 207–216. [CrossRef]
79. Hamieh, T. Some Irregularities in the Evaluation of Surface Parameters of Solid Materials by Inverse Gas Chromatography. *Langmuir* **2023**, *39*, 17059–17070. [CrossRef] [PubMed]
80. Gutmann, V. *The Donor-Acceptor Approach to Molecular Interactions*; Plenum: New York, NY, USA, 1978; 279p.
81. Hamieh, T. The Effect of Temperature on the Surface Energetic Properties of Carbon Fibers Using Inverse Gas Chromatography. *Crystals* **2024**, *14*, 28. [CrossRef]
82. Hamieh, T. New Progress on London Dispersive Energy, Polar Surface Interactions, and Lewis's Acid-Base Properties of Solid Surfaces. *Molecules* **2024**, *29*, 949. [CrossRef]
83. Hamieh, T. London Dispersive and Lewis Acid-Base Surface Energy of 2D Single-Crystalline and Polycrystalline Covalent Organic Frameworks. *Crystals* **2024**, *14*, 148. [CrossRef]
84. Hamieh, T. Inverse Gas Chromatography to Characterize the Surface Properties of Solid Materials. *Chem. Mater.* **2024**, *36*, 2231–2244. [CrossRef]
85. Van Oss, C.J.; Good, R.J.; Chaudhury, M.K. Additive and nonadditive surface tension components and the interpretation of contact angles. *Langmuir* **1988**, *4*, 884. [CrossRef]